THE JOURNAL OF PHYSICAL CHEMISTRY C

Article

Cite This: J. Phys. Chem. C 2019, 123, 4977−4983

pubs.acs.org/JPCC

Ideal Nodal Line Semimetal in a Two-Dimensional Boron Bilayer

Shao-Gang Xu,[†,‡] Baobing Zheng,*[,†,§,∥] Hu Xu,*[,†] and Xiao-Bao Yang*[,‡]

[†]Department of Physics, Southern University of Science and Technology, Shenzhen 518055, P. R. China

[‡]Department of Physics, South China University of Technology, Guangzhou 510640, P. R. China

[§]College of Physics and Optoelectronic Technology, Nonlinear Research Institute, Baoji University of Arts and Sciences, Baoji 721016, P. R. China

[∥]School of Physics and Technology, Wuhan University, Wuhan 430072, P. R. China

Supporting Information

ABSTRACT: The successful experimental syntheses of two-dimensional (2D) boron allotropes with intriguing properties have stimulated great interest in searching for novel low-dimensional boron. By using high-throughput first-principles calculations, we proposed a new stable 2D boron with a bilayer structure ($P\bar{6}$-boron), composed of the building blocks of buckled B_{12} cluster. We showed the possibility of experimental syntheses of $P\bar{6}$-boron on metal substrates and proposed a strategy to pursue for $P\bar{6}$-boron by the B_{12} clusters self-assembly. Specifically, $P\bar{6}$-boron possesses a topologically nontrivial Dirac nodal line, which is protected by the mirror-reflection symmetry. Furthermore, we employed a low-energy effective $\mathbf{k}\cdot\mathbf{p}$ model to prove the existence of the nodal line solution. In addition, the topological analysis of bonding suggests that the chemical bonds of $P\bar{6}$-boron are all covalent rather than ionic bonds found in bilayer $P6/mmm$ boron. We expect that our findings can favor the low-dissipation high-speed nanoelectronic devices based on 2D boron sheets.

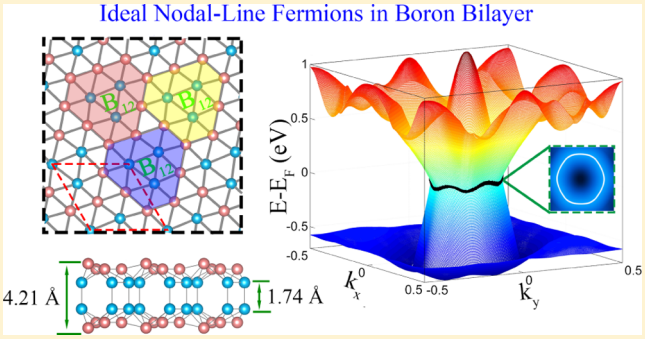

1. INTRODUCTION

Realizing the exotic nontrivial quantum states in practical materials is of great importance in condensed matter physics, such as the typical discoveries of topologically protected Dirac fermions,[1−4] Weyl fermions,[5−7] and node-line femions,[8−12] whose valance band (VB) and conduction band (CB) touch at the discrete points or a continuous closed curve near the Fermi level. These novel electronic states are robust owing to the symmetry protection and provide fascinating transport characteristics, leading to their potential applications in low-power electronic devices.[13−15] Typical topological Dirac fermions can be achieved in the most amazing two-dimensional (2D) material, namely, graphene,[1,16,17] due to its weak spin−orbit coupling.[18] Its massless Dirac fermions, topologically protected by the time-reversal and inversion symmetry,[1,17] provide graphene with extremely high carrier mobility.[16] This unique character is highly desirable in fabricating high-speed nanodevices. Thus, tremendous interests have been made to search for these 2D topological semimetals with exotic properties.

As we know, there are variety of carbon-based nanomaterials, including carbon nanotubes, carbon hollow cages, and planar graphene nanoflakes, and these nanostructures have the same motifs with the graphene sheet due to the stable sp^2 hybridizations of carbon.[1] Distinguished from the carbon element, boron has four possible orbitals while only hosting three valance electrons, which leads to its electron-deficiency behavior. Thus, boron atoms can form a diversity of bonds, ranging from the strongly covalent two-center two-electron (2c−2e) bonds up to metallic-like multicenter bonds.[19] As a result, various boron allotropes are explored, from size-dependent clusters (quasi-planar structures and cage-like borospherenes)[20−22] to three-dimensional (3D) bulk compounds.[23−26] For 2D boron sheets, unlike graphene with a honeycomb lattice, they are stabilized by introducing the extra B atoms in the honeycomb lattice to compensate deficient electrons, forming the expected (2c−2e) bonds up to multicenter two-electron (nc−2e) bonds.[19,27−29] The stabilities of boron monolayers depend on the hexagon vacancy concentration, preferably in the range of 1/9−1/7.[30−33] Owing to their polymorphism, 2D boron allotropes possess rich physical properties. Therefore, great efforts have been paid to these intriguing materials in the last decades, such as the discovery of semiconducting 2D boron monolayers,[34] the possibility of superconductivity in 2D boron allotropes,[35] and the report of 2D magnetic boron.[36] Recently, the topological properties of 2D boron allotropes have received great attention due to the boom of topological materials. The Dirac

Received: December 24, 2018
Revised: January 27, 2019
Published: February 6, 2019

DOI: 10.1021/acs.jpcc.8b12385
J. Phys. Chem. C 2019, 123, 4977−4983

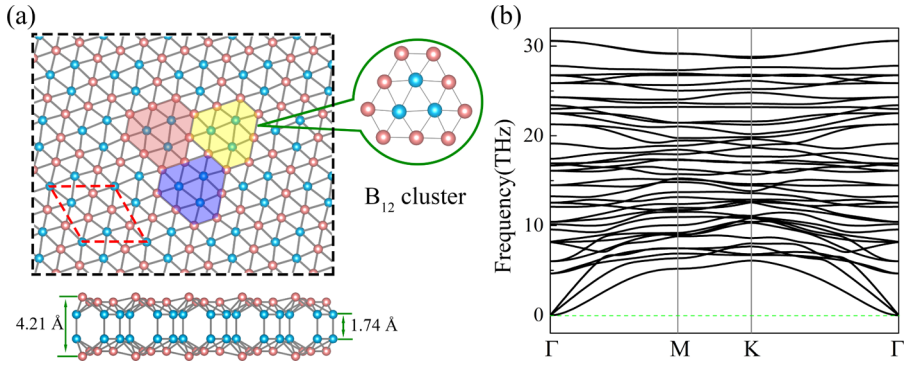

Figure 1. (a) Atomic structure of $P\bar{6}$-boron (top view and side view). (b) The phonon dispersions along the high-symmetry lines of $P\bar{6}$-boron.

fermions[37−41] and the node-line fermions[41,42] are successively predicted in variety of 2D boron allotropes. Interestingly, the Dirac fermions in the β_{12} and χ_3 boron sheets are confirmed by the angle-resolved photoemission spectroscopy measurements.[43,44] However, the hitherto proposed nontrivial fermions in the 2D boron allotropes either are far away from the Fermi level or exist in the energetically unfavorable 2D structures. Therefore, exploring the energetically favorable 2D boron with nontrivial states close to Fermi level is very crucial and essential to date.

Two-dimensional boron allotropes present a diversity of structures, mainly concentrating on the monolayers and bilayers. Previous studies have shown that the bilayer boron sheets are more stable than the monolayers owing to the bond interactions between the adjacent layers.[38,39,45] Therefore, we here primarily focus on the 2D bilayer boron allotropes. In this work, we identified by first-principles calculations a new bilayer boron allotrope with topologically protected node-line fermions. The nodal line is confirmed by the band structure calculations and proved by using a two-band **k·p** model. In addition, we also investigated the type of chemical bonding of the proposed 2D boron.

2. COMPUTATIONAL METHODS

All the first-principles calculations were performed based on density functional theory as implemented in the Vienna ab initio simulation package.[46] The electron−ion interactions were described by the projector-augmented wave method. To treat the exchange−correlation interaction of electrons, we chose the Perdew−Burke−Ernzerhof (PBE) functional within the generalized gradient approximation (GGA).[47] In addition, the accurate Heyd−Scuseria−Ernzerhof screened hybrid functional (HSE06)[48,49] was also employed to confirm the band structure of the 2D boron. The energy cutoff was set to 480 eV, and the forces acting on each atom were less than 0.01 eV/Å. The phonon dispersion curves along the high-symmetry lines were computed by the finite displacement approach as implemented in the phonopy package,[50] where the precision convergence criteria for the total energy was set to 10^{-9} eV to ensure the accuracy of calculations. Thermal stability was also studied using ab initio molecular dynamics (AIMD) simulations with the temperature controlled by a Nosé heat bath scheme.[51] The average formation energies for 2D boron allotropes on the metal substrates are defined in the Supporting Information (SI).

3. RESULTS AND DISCUSSION

To search for the stable boron bilayers with unique topological properties, we performed a global high-throughput structure search[52] based on triangular lattice. This scheme has been demonstrated to be effective and reliable to predict the boron nanostructures.[33,34] The distances between the adjacent layers of the initial structures are set to 1.75 Å, according to the typical covalent bond length of α-boron. There are many stable boron bilayers found in our structure prediction, but we mainly focus on those structures hosting exotic electronic structures. As shown in Figure 1a, our proposed 2D bilayer boron allotrope is constructed by two triangular boron sheets with the layer group of $P\bar{6}$ (no. 74), corresponding to $P\bar{6}$ (no. 174) space group, named $P\bar{6}$-boron. This sandwich-like structure contains two types of boron atoms; the outer boron atoms are 6-fold coordinated, whereas inner boron atoms are 7-fold coordinated due to the bonding between them, with the bond length of 1.74 Å. It is well known that the ground state of B_{12} cluster adopts a quasi-planar structure by fitting an out-of-plane B_3 inner triangle in a B_9 outer ring.[53] Clearly, the B_{12} cluster (the inset of Figure 1a) serves as the building blocks of our predicted $P\bar{6}$-boron with the formation of bond between the B_3 triangles. Thus, it is expected that our proposed $P\bar{6}$-boron would be synthesized by matching the buckled B_{12} cluster together.

The optimized structural parameters and total energies per B atom of $P\bar{6}$-boron are presented in Table 1, together with those of some experimentally and theoretically reported boron sheets for the sake of comparison. Our obtained lattice constants show excellent consistency with the previously reported results,[25,39,42,54,55] suggesting the reliability of our GGA-PBE calculations. The calculated total energy per atom of $P\bar{6}$-boron

Table 1. Lattice Constants, Space Group, and Total Energies E_{tot} for δ_6 Sheet, β_{12} Sheet, χ_3 Sheet, γ_{28} Film, hr-sB, $P6/mmm$, and $P\bar{6}$-Boron

phases	a (Å)	b (Å)	γ (deg)	space group (no.)	E_{tot} (eV/atom)
δ_6[a]	2.87	1.61	90	$Pmmn$(59)	−6.183
β_{12}[b]	2.92	5.07	90	$Pmmm$(47)	−6.230
χ_3[c]	4.45	4.45	38.21	$Cmmm$(65)	−6.243
γ_{28} film[d]	5.62	6.99	90	$P2/m$(10)	−6.164
hr-sB[e]	2.91	8.38	90	$Pmmm$(47)	−6.190
$P6/mmm$[f]	2.86	2.86	120	$P6/mmm$(191)	−6.270
$P\bar{6}$-boron[g]	4.39	4.39	120	$P\bar{6}$(174)	−6.231

[a]Ref 25. [b]Ref 54. [c]Ref 54. [d]Ref 55. [e]Ref 42. [f]Ref 39. [g]This work.

DOI: 10.1021/acs.jpcc.8b12385
J. Phys. Chem. C 2019, 123, 4977−4983

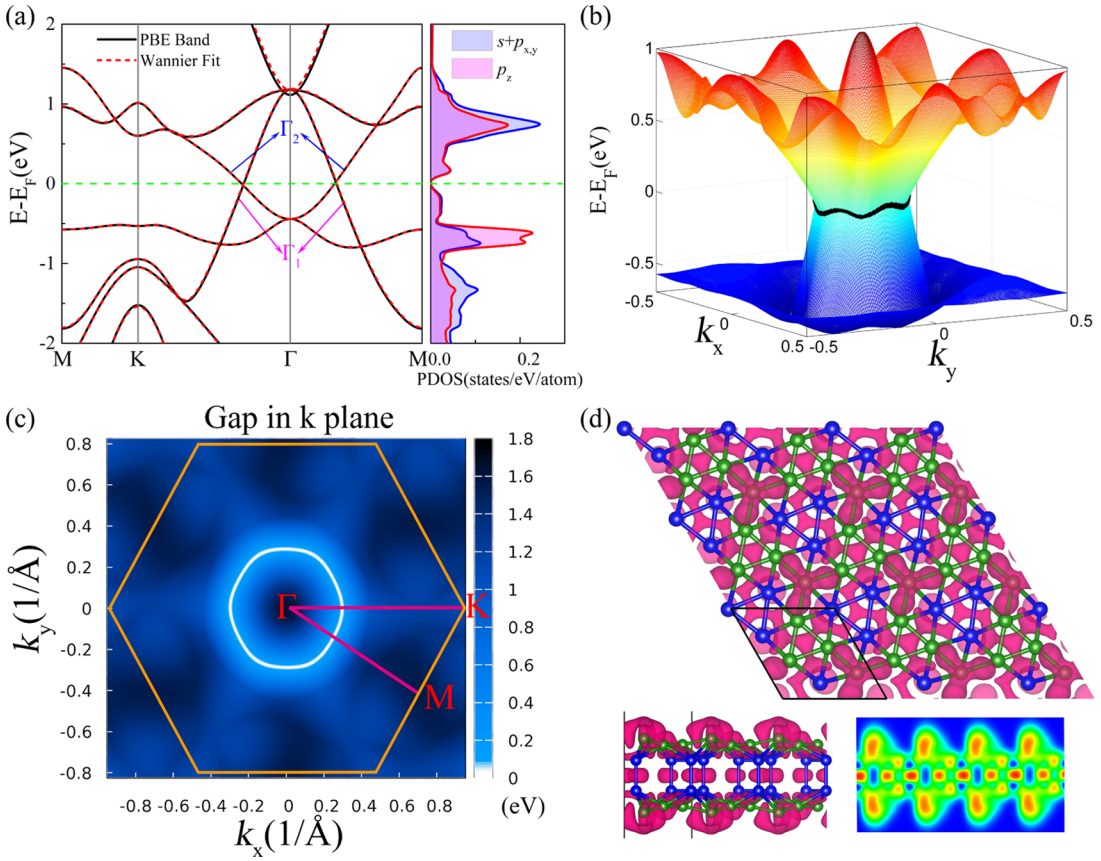

Figure 2. (a) PBE band structures of $P\bar{6}$-boron and the PDOS analysis. (b) Three-dimensional band structures of the VB and CB. (c) Schematic figure of nodal-line cone in the 2D BZ. The color bar indicates the energy difference between CB and VB at each k point. (d) The top and side views of the electron localization function (ELF) of $P6$-boron phase with the isovalue of 0.75.

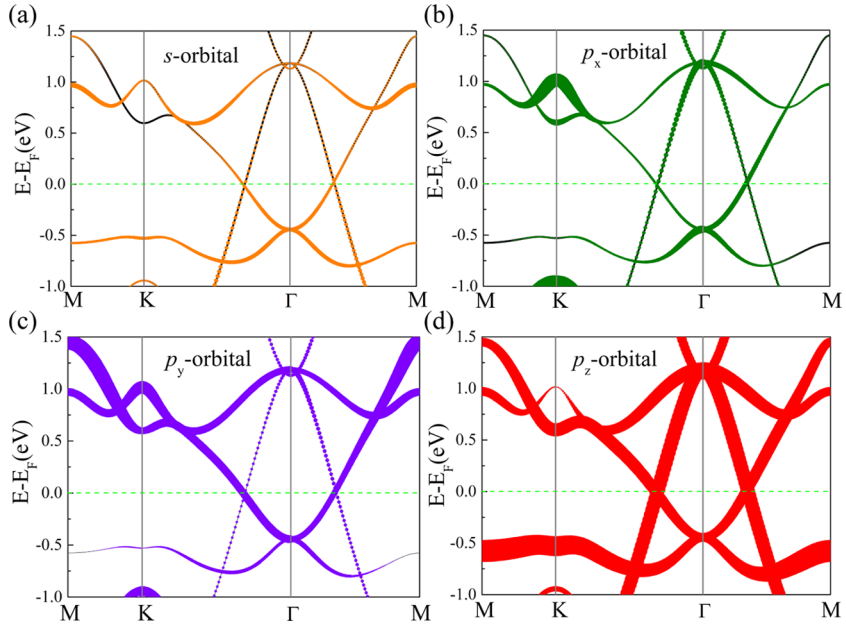

Figure 3. Orbital-resolved band structures of $P\bar{6}$-boron. (a) The orange dots represent the contributions from the s atomic orbital of B atoms; (b) the green, (c) violet, and (d) red dots indicate the contributions of p_x, p_y, and p_z atomic orbitals. Larger dot means higher contribution, whereas smaller one indicates lower contribution.

is slightly larger than that of the predicted $P6/mmm$ phase and comparable to the experimentally synthesized β_{12} and χ_3 phases. Interestingly, $P\bar{6}$-boron has a higher stability than the experimentally reported δ_6 and γ_{28} phases, implying the possibility of experimental syntheses of $P\bar{6}$-boron despite its metastable feature. The dynamical stability of $P\bar{6}$-boron is confirmed by the phonon calculation, as shown in Figure 1b. No imaginary frequencies are found along the high-symmetry

DOI: 10.1021/acs.jpcc.8b12385
J. Phys. Chem. C 2019, 123, 4977−4983

lines in the Brillouin zone, indicating that $P\bar{6}$-boron is dynamically stable. In addition, the thermal stability is verified by the AIMD simulations, the corresponding results are summarized in Figure S1 of the SI.

To further confirm the possibility of its experimental syntheses, we have established different substrates for our predicted $P\bar{6}$-boron. The common metal substrates, such as Au(111), Cu(111), and Ag(111), are considered by controlling the lattice mismatch less than 3%, the corresponding results are illustrated in Figure S2, combined with the results of α-sheet boron,[56] γ_{28} film boron,[55] and *Pmmm* boron[38] for comparison. We also calculated their average formation energies on different substrates, as shown in Figure S3. Clearly, the average formation energies of our predicted $P\bar{6}$-boron are comparable to those of the experimentally reported α-sheet boron[56] and γ_{28} film,[55] further indicating the possible syntheses of $P\bar{6}$-boron on these metal substrates by choosing suitable growth condition. Specifically, our proposed $P\bar{6}$-boron may be prepared by the self-assembly of B_{12} clusters in view of its basic building-block of B_{12} clusters, which is similar to the realization of graphene.[57]

To study the topological properties, we first calculated the band structures and projected density of states (PDOS) of $P\bar{6}$-boron, as shown in Figure 2a. Clearly, $P\bar{6}$-boron exhibits zero-gap semimetallic feature. Along $K-\Gamma$ and $\Gamma-M$ lines, the valence band (VB) and conduction band (CB) linearly cross at two points and form two Dirac points at the Fermi level. The linear dispersions near the two Dirac points reveal that the effective mass of carrier for $P\bar{6}$-boron, defined by $m^* = \hbar^2/\frac{\partial^2 E}{\partial k^2}$, is zero, suggesting its extremely high carrier mobility. The slope of band around the Fermi level in the $K-\Gamma$ direction is 33.5 eV Å (−12.7 eV Å) and the corresponding Fermi velocity ($v_f = \partial E/\hbar\partial k$) is 0.81×10^6 m/s (0.31×10^6 m/s), comparable to that of graphene (0.82×10^6 m/s).[37] Along the $\Gamma-M$ direction, the slope of band is 16.7 eV Å (−33.5 eV Å) and v_f is 0.40×10^6 m/s (0.81×10^6 m/s). The anisotropic Dirac cone with different slopes along different directions indicates direction-dependent electronic properties of $P\bar{6}$-boron.

To gain a deeper insight into the origin of the Dirac cone, we calculated the orbital-resolved band structures of $P\bar{6}$-boron (see Figure 3). Different from the Dirac cone of graphene, the two crossing bands mainly arise from the out-of-plane p_z states, but the in-plane sp^2 hybrid states, composed of s, p_x, and p_y orbitals, also contribute partially for the formation of Dirac cone along the high-symmetry lines. Furthermore, the PDOS in Figure 2a further confirms the above results. Based on the basis set of sp^2 and p_z orbitals, we calculated the band structures of $P\bar{6}$-boron (red dashed line in Figure 2a) by using a tight-binding Hamiltonian with maximally localized Wannier functions.[58,59] The obtained band structures fit well with the GGA-PBE results, revealing that the Dirac cone in $P\bar{6}$-boron is indeed attributed by the combination of the sp^2 and p_z orbitals rather than sole p_z orbitals.

Further 3D representation of band structures (Figure 2b) in the vicinity of the Dirac points show that the VB and CB linearly cross in all directions around the Fermi level and thus result in a closed ring around the Γ point in the first Brillouin zone, namely, the node-line fermions. The nodal line of $P\bar{6}$-boron also can be clearly observed in the contour plot of the energy gap between the VB and CB (see Figure 2c). To check the robustness of the nodal line, we applied the in-plane biaxial strain (±5%) for $P\bar{6}$-boron. The obtained GGA-PBE results reveal that these structure distortions with preservation of symmetries only slightly shift the positions of band-crossings near the Fermi level, but the linear band-crossings still hold (see Figure S4a,b), suggesting the node-line is robust. Moreover, the high-precision HSE06 calculations also support the above conclusions, as shown in Figure S4c. Because of the light mass of boron, spin−orbit coupling has a negligible influence on the band-crossings of $P\bar{6}$-boron, and merely opens an extremely small band gap less than 1 meV (Figure S4d).

Symmetry analysis can provide a fundamental understanding of the study of the nontrivial electronic states. Therefore, we next investigate the nodal line from the viewpoint of symmetry. $P\bar{6}$-boron has the symmorphic C_{3h}^1 space group (no. 174), in which the mirror-reflection symmetry (M_z) is present. Thus, all momentum points host the little group C_s in the 2D Brillouin zone. The two linearly cross bands belong to the different irreducible representation (IR) Γ_1 and Γ_2 of C_s, with opposite mirror eigenvalues of 1 and −1. An inspection of IR of the two bands reveals that the ordering of the CB and VB is inverted, forming a continuous nodal-ring around the Γ point. This is responsible for the existence of this topological nontrivial state. In general, the two inverted bands can be described by a two-band $\mathbf{k}\cdot\mathbf{p}$ Hamiltonian

$$H(\mathbf{k}) = \sum_{i=0}^{3} d_i(\mathbf{k})\sigma_i \tag{1}$$

where d_0 is a kinetic term that is irrelevant to band-crossings and hence has been ignored in the following, σ_0 is a 2×2 identity matrix, $\sigma_{1,2,3}$ represent the Pauli matrices, $d_{1,2,3}(\mathbf{k})$ are real functions, and $\mathbf{k} = (k_x, k_y)$ are the two components of the momentum $\mathbf{k}$. Consider the opposite mirror eigenvalues (± 1) of the mirror-reflection symmetry, M_z may be represented by $M_z = \sigma_z$. The mirror-reflection symmetry indicates that

$$M_z H(k_x, k_y) M_z^{-1} = H(k_x, k_y) \tag{2}$$

which can be reduced to

$$d_{1,2}(k_x, k_y) = -d_{1,2}(-k_x, -k_y),\ d_3(k_x, k_y) = d_3(-k_x, -k_y) \tag{3}$$

Equation 3 implies that

$$d_{1,2}(k_x, k_y) = 0,\ \ d_3(k_x, k_y) \neq 0 \tag{4}$$

The energy dispersion of eq 1 is thus obtained as

$$E = \pm|d_3(k_x, k_y)| \tag{5}$$

From eq 5, the band-crossing only occurs when $d_3(\mathbf{k})$ equals to zero, which has co-dimension one, thus allowing a nodal line in momentum space.

The ionic boron in the bulk phase was first reported at high pressure,[60] and subsequently predicted in 2D at ambient pressure.[39] Owing to the bilayer structure of $P\bar{6}$-boron, which is slightly similar to that of the proposed ionic 2D boron, we thus studied the type of chemical bonds of $P\bar{6}$-boron fundamentally to determine whether the ionic bond exists in $P\bar{6}$-boron. The electron localization function (ELF) of $P\bar{6}$-boron with the isovalue of 0.75 (a critical value to identify the covalent bond) is illustrated in Figure 2d. The emergence of high electron localizations evidently between boron atoms implies the formation of a covalent bond in $P\bar{6}$-boron. To further check the covalent feature of $P\bar{6}$-boron, we performed the topological analysis of bonding based on the atoms-in-

DOI: 10.1021/acs.jpcc.8b12385
J. Phys. Chem. C 2019, 123, 4977−4983

molecules theory proposed by Bader.[61] The estimated Bader charge transfers are very slight, approximately 0.1−0.3*e* for different boron atoms, characteristic of primarily covalent bond in $P\bar{6}$-boron. In addition, the bond critical points (BCPs) can distinguish between the covalent bond and ionic bond, according to the Laplacian of charge density (LCD) at the critical points. As listed in Table 2, the largest charge density

Table 2. Averages of Bond Lengths R_{av}, Electronic Densities ρ_{av}, Laplacians of Charge Densities $(\nabla^2\rho)_{av}$ at the (3,−1) Bond Critical Point for $P\bar{6}$-Boron, the Units of ρ_{av} and $(\nabla^2\rho)_{av}$ Are au[a]

B atom type	type of bonding	R_{av} (Å)	ρ_{av}	$(\nabla^2\rho)_{av}$
inner B atoms	with inner B atoms between the B_3 triangle	1.737	0.141	−0.271
inner B atoms	with inner B atoms in the B_3 triangle	1.832	0.102	−0.060
inner B atoms	with outer B atoms	1.777	0.116	−0.099
outer B atoms	with outer B atoms	1.691	0.130	−0.156

[a]The large charge densities and negative Laplacians indicate a covalent bond, otherwise a noncovalent bond.

and the relatively negative LCD at the BCPs support the covalent interaction between the adjacent inner boron atoms. Moreover, for the bonds between the inner boron atoms and the adjacent outer boron atoms, the average LCD presents a slightly negative value, indicating their covalent behaviors despite weak covalency. Therefore, we can conclude that the chemical bonds of $P\bar{6}$-boron are covalent rather than ionic as in ionic 2D boron.

4. CONCLUSIONS

In summary, we proposed a new stable sandwich boron sheet, namely, $P\bar{6}$-boron, in which the buckled B_{12} cluster serves as the building block. The dynamical and thermal stabilities of $P\bar{6}$-boron are checked by the phonon calculations and AIMD simulations. We also established the metal substrates for our predicted $P\bar{6}$-boron, and the results suggest its possible experimental syntheses by B_{12} clusters self-assembly. The band structures show that $P\bar{6}$-boron hosts the Dirac points along high symmetry lines, with the Fermi velocity of $\sim 10^6$ m/s comparable to that of graphene. Further 3D representation of band structures indicates that it is a Dirac nodal-line in the 2D Brillouin zone, which is protected by the mirror symmetry. Moreover, we employed a low-energy effective **k·p** model to show the node-line solution. In addition, no ionic bonds emerge in our bilayer $P\bar{6}$-boron, according to the topological analysis of bonding.

■ ASSOCIATED CONTENT

Supporting Information

The Supporting Information is available free of charge on the ACS Publications website at DOI: 10.1021/acs.jpcc.8b12385.

AIMD simulation results; adsorption on the metal substrates; calculation of average formation energies; band structures of $P\bar{6}$-boron (PDF)

■ AUTHOR INFORMATION

Corresponding Authors

*E-mail: scu_zheng@163.com (B.Z.).
*E-mail: xu.h@sustc.edu.cn (H.X.).
*E-mail: scxbyang@scut.edu.cn (X.-B.Y.).

ORCID

Baobing Zheng: 0000-0003-4292-1556
Hu Xu: 0000-0002-2254-5840
Xiao-Bao Yang: 0000-0001-8851-1988

Notes

The authors declare no competing financial interest.

■ ACKNOWLEDGMENTS

This work was supported by the National Natural Science Foundation of China (NSFC, Grant Nos. 11674148, 11334003, 11404159, and 11474100), the Guangdong Natural Science Funds for Distinguished Young Scholars (Nos. 2014A030306024 and 2017B030306008), the Natural Science Basic Research plan in Shaanxi Province of China (Grant No. 2018JQ1083), the Scientific Research Program Funded by Shaanxi Provincial Education Department (Grant No. 17JK0041), the Baoji University of Arts and Sciences Key Research (Grant No. ZK2017009), and the Center for Computational Science and Engineering of Southern University of Science and Technology.

■ REFERENCES

(1) Castro Neto, A. H.; Guinea, F.; Peres, N. M. R.; Novoselov, K. S.; Geim, A. K. The Electronic Properties of Graphene. *Rev. Mod. Phys.* **2009**, *81*, 109−162.
(2) Liu, Z. K.; Zhou, B.; Zhang, Y.; Wang, Z. J.; Weng, H. M.; Prabhakaran, D.; Mo, S.-K.; Shen, Z. X.; Fang, Z.; Dai, X.; et al. Discovery of a Three-Dimensional Topological Dirac Semimetal, Na_3bi. *Science* **2014**, *343*, 864−867.
(3) Wang, Z.; Sun, Y.; Chen, X.-Q.; Franchini, C.; Xu, G.; Weng, H.; Dai, X.; Fang, Z. Dirac Semimetal and Topological Phase Transitions in A_3bi (a = Na, K, Rb). *Phys. Rev. B* **2012**, *85*, No. 195320.
(4) Wang, Z.; Weng, H.; Wu, Q.; Dai, X.; Fang, Z. Three-Dimensional Dirac Semimetal and Quantum Transport in Cd_3as_2. *Phys. Rev. B* **2013**, *88*, No. 125427.
(5) Wan, X.; Turner, A. M.; Vishwanath, A.; Savrasov, S. Y. Topological Semimetal and Fermi-Arc Surface States in the Electronic Structure of Pyrochlore Iridates. *Phys. Rev. B* **2011**, *83*, No. 205101.
(6) Xu, G.; Weng, H.; Wang, Z.; Dai, X.; Fang, Z. Chern Semimetal and the Quantized Anomalous Hall Effect in $Hgcr_2se_4$. *Phys. Rev. Lett.* **2011**, *107*, No. 186806.
(7) Weng, H.; Fang, C.; Fang, Z.; Bernevig, B. A.; Dai, X. Weyl Semimetal Phase in Noncentrosymmetric Transition-Metal Monophosphides. *Phys. Rev. X* **2015**, *5*, No. 011029.
(8) Burkov, A. A.; Hook, M. D.; Balents, L. Topological Nodal Semimetals. *Phys. Rev. B* **2011**, *84*, No. 235126.
(9) Yu, R.; Weng, H.; Fang, Z.; Dai, X.; Hu, X. Topological Node-Line Semimetal and Dirac Semimetal State in Antiperovskite Cu_3PdN. *Phys. Rev. Lett.* **2015**, *115*, No. 036807.
(10) Kim, Y.; Wieder, B. J.; Kane, C. L.; Rappe, A. M. Dirac Line Nodes in Inversion-Symmetric Crystals. *Phys. Rev. Lett.* **2015**, *115*, No. 036806.
(11) Mullen, K.; Uchoa, B.; Glatzhofer, D. T. Line of Dirac Nodes in Hyperhoneycomb Lattices. *Phys. Rev. Lett.* **2015**, *115*, No. 026403.
(12) Weng, H.; Liang, Y.; Xu, Q.; Yu, R.; Fang, Z.; Dai, X.; Kawazoe, Y. Topological Node-Line Semimetal in Three-Dimensional Graphene Networks. *Phys. Rev. B* **2015**, *92*, No. 045108.
(13) Hosur, P.; Parameswaran, S. A.; Vishwanath, A. Charge Transport in Weyl Semimetals. *Phys. Rev. Lett.* **2012**, *108*, No. 046602.

DOI: 10.1021/acs.jpcc.8b12385
J. Phys. Chem. C 2019, 123, 4977−4983

(14) Kim, H.-J.; Kim, K.-S.; Wang, J. F.; Sasaki, M.; Satoh, N.; Ohnishi, A.; Kitaura, M.; Yang, M.; Li, L. Dirac Versus Weyl Fermions in Topological Insulators: Adler-Bell-Jackiw Anomaly in Transport Phenomena. *Phys. Rev. Lett.* **2013**, *111*, No. 246603.
(15) Armitage, N. P.; Mele, E. J.; Vishwanath, A. Weyl and Dirac Semimetals in Three-Dimensional Solids. *Rev. Mod. Phys.* **2018**, *90*, No. 015001.
(16) Geim, A. K.; Novoselov, K. S. The Rise of Graphene. *Nat. Mater.* **2007**, *6*, 183.
(17) Novoselov, K. S.; Geim, A. K.; Morozov, S. V.; Jiang, D.; Katsnelson, M. I.; Grigorieva, I. V.; Dubonos, S. V.; Firsov, A. A. Two-Dimensional Gas of Massless Dirac Fermions in Graphene. *Nature* **2005**, *438*, 197.
(18) Yao, Y.; Ye, F.; Qi, X.-L.; Zhang, S.-C.; Fang, Z. Spin-Orbit Gap of Graphene: First-Principles Calculations. *Phys. Rev. B* **2007**, *75*, No. 041401.
(19) Sergeeva, A. P.; Popov, I. A.; Piazza, Z. A.; Li, W.-L.; Romanescu, C.; Wang, L.-S.; Boldyrev, A. I. Understanding Boron through Size-Selected Clusters: Structure, Chemical Bonding, and Fluxionality. *Acc. Chem. Res.* **2014**, *47*, 1349−1358.
(20) Alexandrova, A. N.; Boldyrev, A. I.; Zhai, H.-J.; Wang, L.-S. All-Boron Aromatic Clusters as Potential New Inorganic Ligands and Building Blocks in Chemistry. *Coord. Chem. Rev.* **2006**, *250*, 2811−2866.
(21) Zhai, H.-J.; Zhao, Y.-F.; Li, W.-L.; Chen, Q.; Bai, H.; Hu, H.-S.; Piazza, Z. A.; Tian, W.-J.; Lu, H.-G.; Wu, Y.-B.; et al. Observation of an All-Boron Fullerene. *Nat. Chem.* **2014**, *6*, 727.
(22) Wang, L.-S. Photoelectron Spectroscopy of Size-Selected Boron Clusters: From Planar Structures to Borophenes and Borospherenes. *Int. Rev. Phys. Chem.* **2016**, *35*, 69−142.
(23) Huang, W.; Sergeeva, A. P.; Zhai, H.-J.; Averkiev, B. B.; Wang, L.-S.; Boldyrev, A. I. A Concentric Planar Doubly Π-Aromatic B19− Cluster. *Nat. Chem.* **2010**, *2*, 202.
(24) Bezugly, V.; Kunstmann, J.; Grundkötter-Stock, B.; Frauenheim, T.; Niehaus, T.; Cuniberti, G. Highly Conductive Boron Nanotubes: Transport Properties, Work Functions, and Structural Stabilities. *ACS Nano* **2011**, *5*, 4997−5005.
(25) Mannix, A. J.; Zhou, X.-F.; Kiraly, B.; Wood, J. D.; Alducin, D.; Myers, B. D.; Liu, X.; Fisher, B. L.; Santiago, U.; Guest, J. R.; et al. Synthesis of Borophenes: Anisotropic, Two-Dimensional Boron Polymorphs. *Science* **2015**, *350*, 1513−1516.
(26) Decker, B. F.; Kasper, J. S. The Crystal Structure of a Simple Rhombohedral Form of Boron. *Acta Crystallogr.* **1959**, *12*, 503−506.
(27) Chen, Q.; Wei, G.-F.; Tian, W.-J.; Bai, H.; Liu, Z.-P.; Zhai, H.-J.; Li, S.-D. Quasi-Planar Aromatic B_{36} and B_{36}^- Clusters: All-Boron Analogues of Coronene. *Phys. Chem. Chem. Phys.* **2014**, *16*, 18282−18287.
(28) Li, R.; You, X.-R.; Wang, K.; Zhai, H.-J. Nature of Bonding in Bowl-Like B_{36} Cluster Revisited: Concentric (6π + 18π) Double Aromaticity and Reason for the Preference of a Hexagonal Hole in a Central Location. *Chem. - Asian J.* **2018**, *13*, 1148−1156.
(29) Zhang, Z.; Penev, E. S.; Yakobson, B. I. Polyphony in B Flat. *Nat. Chem.* **2016**, *8*, 525.
(30) Tang, H.; Ismail-Beigi, S. Novel Precursors for Boron Nanotubes: The Competition of Two-Center and Three-Center Bonding in Boron Sheets. *Phys. Rev. Lett.* **2007**, *99*, No. 115501.
(31) Yang, X.; Ding, Y.; Ni, J. Ab Initio Prediction of Stable Boron Sheets and Boron Nanotubes: Structure, Stability, and Electronic Properties. *Phys. Rev. B* **2008**, *77*, No. 041402.
(32) Penev, E. S.; Bhowmick, S.; Sadrzadeh, A.; Yakobson, B. I. Polymorphism of Two-Dimensional Boron. *Nano Lett.* **2012**, *12*, 2441−2445.
(33) Xu, S.-G.; Li, X.-T.; Zhao, Y.-J.; Liao, J.-H.; Xu, H.; Yang, X.-B. An Electron Compensation Mechanism for the Polymorphism of Boron Monolayers. *Nanoscale* **2018**, *10*, 13410−13416.
(34) Xu, S.-G.; Li, X.-T.; Zhao, Y.-J.; Liao, J.-H.; Xu, W.-P.; Yang, X.-B.; Xu, H. Two-Dimensional Semiconducting Boron Monolayers. *J. Am. Chem. Soc.* **2017**, *139*, 17233−17236.
(35) Penev, E. S.; Kutana, A.; Yakobson, B. I. Can Two-Dimensional Boron Superconduct? *Nano Lett.* **2016**, *16*, 2522−2526.
(36) Zhou, X.-F.; Oganov, A. R.; Wang, Z.; Popov, I. A.; Boldyrev, A. I.; Wang, H.-T. Two-Dimensional Magnetic Boron. *Phys. Rev. B* **2016**, *93*, No. 085406.
(37) Jiao, Y.; Ma, F.; Bell, J.; Bilic, A.; Du, A. Two-Dimensional Boron Hydride Sheets: High Stability, Massless Dirac Fermions, and Excellent Mechanical Properties. *Angew. Chem., Int. Ed.* **2016**, *55*, 10292−10295.
(38) Zhou, X.-F.; Dong, X.; Oganov, A. R.; Zhu, Q.; Tian, Y.; Wang, H.-T. Semimetallic Two-Dimensional Boron Allotrope with Massless Dirac Fermions. *Phys. Rev. Lett.* **2014**, *112*, No. 085502.
(39) Ma, F.; Jiao, Y.; Gao, G.; Gu, Y.; Bilic, A.; Chen, Z.; Du, A. Graphene-Like Two-Dimensional Ionic Boron with Double Dirac Cones at Ambient Condition. *Nano Lett.* **2016**, *16*, 3022−3028.
(40) Yi, W.-c.; Liu, W.; Botana, J.; Zhao, L.; Liu, Z.; Liu, J.-y.; Miao, M.-s. Honeycomb Boron Allotropes with Dirac Cones: A True Analogue to Graphene. *J. Phys. Chem. Lett.* **2017**, *8*, 2647−2653.
(41) Gupta, S.; Kutana, A.; Yakobson, B. I. Dirac Cones and Nodal Line in Borophene. *J. Phys. Chem. Lett.* **2018**, *9*, 2757−2762.
(42) Zhang, H.; Xie, Y.; Zhang, Z.; Zhong, C.; Li, Y.; Chen, Z.; Chen, Y. Dirac Nodal Lines and Tilted Semi-Dirac Cones Coexisting in a Striped Boron Sheet. *J. Phys. Chem. Lett.* **2017**, *8*, 1707−1713.
(43) Feng, B.; Zhang, J.; Ito, S.; Arita, M.; Cheng, C.; Chen, L.; Wu, K.; Komori, F.; Sugino, O.; Miyamoto, K.; et al. Discovery of 2d Anisotropic Dirac Cones. *Adv. Mater.* **2017**, *30*, No. 1704025.
(44) Feng, B.; Sugino, O.; Liu, R.-Y.; Zhang, J.; Yukawa, R.; Kawamura, M.; Iimori, T.; Kim, H.; Hasegawa, Y.; Li, H.; et al. Dirac Fermions in Borophene. *Phys. Rev. Lett.* **2017**, *118*, No. 096401.
(45) Zhao, Y.; Zeng, S.; Ni, J. Superconductivity in Two-Dimensional Boron Allotropes. *Phys. Rev. B* **2016**, *93*, No. 014502.
(46) Kresse, G.; Furthmuller, J. Efficient Iterative Schemes for Ab Initio Total-Energy Calculations Using a Plane-Wave Basis Set. *Phys. Rev. B* **1996**, *54*, 11169−11186.
(47) Perdew, J. P.; Burke, K.; Ernzerhof, M. Generalized Gradient Approximation Made Simple. *Phys. Rev. Lett.* **1996**, *77*, 3865−3868.
(48) Heyd, J.; Scuseria, G. E.; Ernzerhof, M. Hybrid Functionals Based on a Screened Coulomb Potential. *J. Chem. Phys.* **2003**, *118*, 8207−8215.
(49) Paier, J.; Marsman, M.; Hummer, K.; Kresse, G.; Gerber, I. C.; Ángyán, J. G. Screened Hybrid Density Functionals Applied to Solids. *J. Chem. Phys.* **2006**, *124*, No. 154709.
(50) Togo, A.; Oba, F.; Tanaka, I. First-Principles Calculations of the Ferroelastic Transition between Rutile-type and $CaCl_2$-type SiO_2 at High Pressures. *Phys. Rev. B* **2008**, *78*, No. 134106.
(51) Nosé, S. A Unified Formulation of the Constant Temperature Molecular Dynamics Methods. *J. Chem. Phys.* **1984**, *81*, 511−519.
(52) Li, X.-T.; Xu, S.-G.; Yang, X.-B.; Zhao, Y.-J. An Intrinsic Representation of Atomic Structure: From Clusters to Periodic Systems. *J. Chem. Phys.* **2017**, *147*, No. 144106.
(53) Zhai, H.-J.; Kiran, B.; Li, J.; Wang, L.-S. Hydrocarbon Analogues of Boron Clusters — Planarity, Aromaticity and Antiaromaticity. *Nat. Mater.* **2003**, *2*, 827.
(54) Feng, B.; Zhang, J.; Zhong, Q.; Li, W.; Li, S.; Li, H.; Cheng, P.; Meng, S.; Chen, L.; Wu, K. Experimental Realization of Two-Dimensional Boron Sheets. *Nat. Chem.* **2016**, *8*, 563.
(55) Tai, G.; Hu, T.; Zhou, Y.; Wang, X.; Kong, J.; Zeng, T.; You, Y.; Wang, Q. Synthesis of Atomically Thin Boron Films on Copper Foils. *Angew. Chem., Int. Ed.* **2015**, *54*, 15473−15477.
(56) Zhong, Q.; Jin, Z.; Peng, C.; Baojie, F.; Wenbin, L.; Shaoxiang, S.; Hui, L.; Sheng, M.; Lan, C.; Kehui, W. Metastable Phases of 2d Boron Sheets on Ag(1 1 1). *J. Phys.: Condens. Matter* **2017**, *29*, No. 095002.
(57) Ciesielski, A.; Samorì, P. Supramolecular Approaches to Graphene: From Self-Assembly to Molecule-Assisted Liquid-Phase Exfoliation. *Adv. Mater.* **2016**, *28*, 6030−6051.
(58) Marzari, N.; Mostofi, A. A.; Yates, J. R.; Souza, I.; Vanderbilt, D. Maximally Localized Wannier Functions: Theory and Applications. *Rev. Mod. Phys.* **2012**, *84*, 1419−1475.

DOI: 10.1021/acs.jpcc.8b12385
J. Phys. Chem. C 2019, 123, 4977−4983

(59) Mostofi, A. A.; Yates, J. R.; Pizzi, G.; Lee, Y.-S.; Souza, I.; Vanderbilt, D.; Marzari, N. An Updated Version of Wannier90: A Tool for Obtaining Maximally-Localised Wannier Functions. *Comput. Phys. Commun.* **2014**, *185*, 2309−2310.
(60) Oganov, A. R.; Chen, J.; Gatti, C.; Ma, Y.; Ma, Y.; Glass, C. W.; Liu, Z.; Yu, T.; Kurakevych, O. O.; Solozhenko, V. L. Ionic High-Pressure Form of Elemental Boron. *Nature* **2009**, *457*, 863.
(61) Bader, R. F. W. *Atoms in Molecules: A Quantum Theory*; Oxford University Press: Oxford, England, 1990.

DOI: 10.1021/acs.jpcc.8b12385
J. Phys. Chem. C 2019, 123, 4977−4983